SUPPLEMENTARY INFORMATION

# A Nanoscale Parametric Feedback Oscillator

L.G. Villanueva, R.B. Karabalin, M.H. Matheny, E. Kenig, M.C. Cross, M.L. Roukes

Kavli Nanoscience Institute, California Institute of Technology, Pasadena, CA, 91125

correspondence to: roukes@caltech.edu

I.   Fabrication process flow

The fabrication of our devices is very similar to the one already reported[S1]. It is performed on dices of a silicon wafer that has been prepared with a 2 μm thick layer of SiO_2, 20 nm thick AlN seed layer, 100 nm thick Mo, 50 nm thick AlN active layer and 40 nm thick Mo. Fig. S1 shows an schematic representation of the process flow. We start by patterning the top Mo layer to define some mesas that are later used for the mechanical devices. We do that depositing an Al thin layer via lift-off with PMMA and performing a dry etching of Mo with SF_6 (Fig. S1.a). KOH is used to remove Al and AlN simultaneously using Mo as a mask for the latter (Fig. S1.b). We perform a dry etch of the two Mo layers in order to define electrical paths, actuation electrodes and piezometallic loops for detection. We do this in a two steps process using ZEP as a mask and SF_6 as the etching species (Fig. S1.c). We later pattern the mechanical devices using a strontium fluoride (SrF_2) mask and chlorine dry etching of the stack (Fig. S1.d). In order to contact the top Mo on the mechanical devices, we deposit SrF_2 isolation "bridges" and, subsequently, we perform a lift-off of Au, also defining our contact pads (Fig. S1.e). We finally release the mechanical structures via a wet etching using buffered HF (Fig. S1.f).
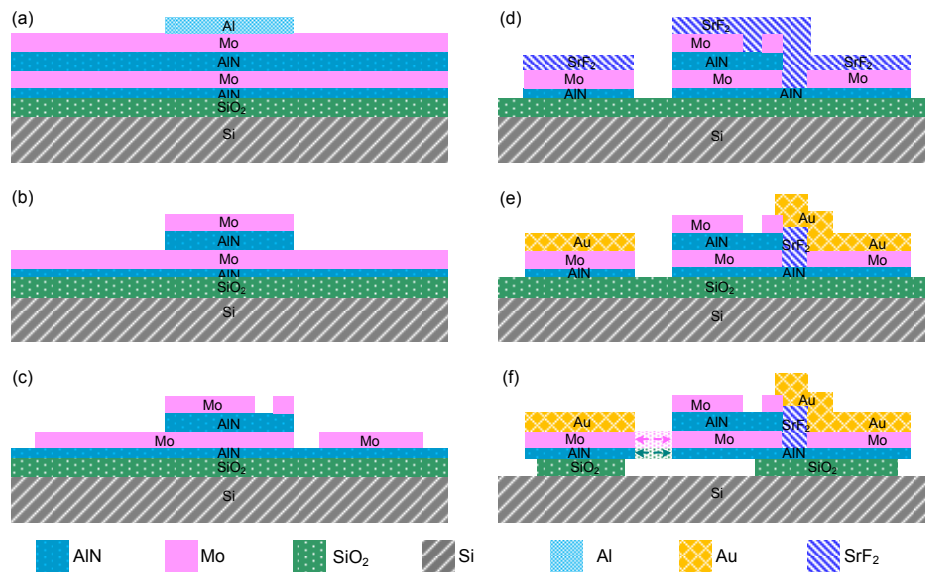
Fig. S1 | Fabrication process flow. Surface nanomachining process flow for piezoelectric AlN NEMS. a) Definition of mesa, followed by a dry etch of Mo. b) KOH wet etching of AlN and Al mask. c) Patterning of top and bottom Mo to define electrodes and transduction structures (actuation and detection). d) Definition of the mechanical structures via dry etching of the four-layered stack. e) Insulating bridges in SrF_2 are deposited, followed by Au deposition to define contact pads and to contact top Mo. f) Release of mechanical structures using BHF wet etching.

II.   Theoretical analysis of the PFO

To analyze the behavior of equation (1) from the main text, it is convenient to focus on the slow modulations of the resonator oscillations. We follow the approach reviewed elsewhere[S2]. The displacement of the beam is given in terms of a slowly varying complex modulation function or amplitude $A(t)$ by:

$$x(t) \propto A(t)e^{i\omega_0 t} + c.c. + \cdots \tag{S1}$$

with ω_0 the resonant frequency of the beam. The $\cdots$ in Eq. (S1) represent higher harmonics which will be small for the range of oscillation amplitudes we need to consider, and will be neglected from hereon. The squared, amplified, filtered around 2f, phase shifted feedback signal is

$$\tilde{F} = F(|A|^2)A^2 e^{i\Delta} e^{i2\omega_0 t} + c.c. \tag{S2}$$

with $F(y)$ the gain function of the amplifier filter circuit that we take to be

$$F(y) = \frac{\Gamma}{1 + \left(\frac{\Gamma}{s}\right)y} \tag{S3}$$

This gives a linear gain Γ of the squared signal at small amplitudes, and at large amplitudes $F(y) \to s/y$ so that the feedback signal takes on the saturated value

$$\tilde{F} = s \cdot e^{i(\theta(T)+\Delta)} e^{i2\omega_0 t} + c.c. \tag{S4}$$

with θ the phase of A and s the saturation amplitude of the amplifier. The feedback is applied multiplicatively to the displacement of the beam. Keeping the resonant terms at $e^{i\omega_0 t}$ gives the amplitude equation describing the resonator and parametric feedback system

$$\frac{dA}{dT} = -\frac{1}{2}A + \frac{1}{8}\left[F(|A|^2)ie^{i\Delta} + 3i - \eta\right]|A|^2 A \tag{S5}$$

Here we have introduced the slow scaled time $T = \omega_0 t/Q$ so that times are measured in units of the inverse line width of the linear resonator. The term $-\frac{1}{2}A$ on the right hand side of Eq. (S5) is the linear decay rate of undriven oscillations in the resonator in these units. The proportionality constant in Eq. (S1) is chosen so that the frequency shift due to the nonlinearity in the resonator is $\frac{3}{8}|A|^2\omega_0/Q$ which means that the amplitude for the onset of bistability in the driven response of the resonator is $|A|_c^2 = \frac{8}{3}\frac{1}{\sqrt{3}-\eta}$. The term depending on η arises from the nonlinear dissipation. For a system with direct sinusoidal drive, such as to initiate the oscillations or the setup studied in Fig. 2 there would be an additional term on the right hand side of Eq. (S5): $ge^{i\Omega T}$ with Ω being the frequency of the drive relative to the linear resonant frequency expressed in units of the resonance linewidth.

For small amplitudes of feedback, the gain function will be in the linear regime. In this case the nonlinear term in Eq. (S5) becomes:

$$\frac{1}{8}\left[i(3 + F(|A|^2)\cos(\Delta)) - (\eta + F(|A|^2)\sin(\Delta))\right]|A|^2 A \qquad \text{(S6)}$$

so that the feedback circuit can be used to tune either the nonlinear frequency pulling or the nonlinear dissipation of the resonator depending on the choice of feedback phase Δ, as demonstrated in Fig. 2.

For sufficiently strong feedback, Eq. (S5) supports sustained oscillations. Although it is straightforward to solve the equation in general, in the experimental setup once the oscillations develop the feedback system is almost always in the limit of saturated gain function, and so we illustrate the results for this case. This corresponds to setting $F(|A|^2)|A|^2 \rightarrow s$. Note that this corresponds to parametric drive with fixed amplitude, as in usual parametric experiments, but with a phase given by the signal phase plus the additional phase from the feedback loop. Of course in the present case, the parametric drive comes from the feedback of the amplified output of the resonator, and not from an external a.c. drive signal.

For self-sustained oscillations we set $A(T) = a(T)e^{i\theta(T)}$ and use Eq. (S5) to find equations for the amplitude and phase

$$\frac{da}{dT} = -a\left(\frac{1}{2} + \frac{1}{8}s\,sin(\Delta)\right) - \frac{1}{8}\eta a^3 \qquad \text{(S7)}$$

$$\frac{d\theta}{dT} = \frac{1}{8}s\cos(\Delta) + \frac{3}{8}a^2 \qquad \text{(S8)}$$

Note that the term amplifying the magnitude is proportional to $s\sin(\Delta)$, so that for some values of Δ and for large enough s, the feedback gain can overcome the linear dissipation and can bring the system into oscillation. For steady state oscillations $\frac{da}{dT} = 0$, $\frac{d\theta}{dT} = \Omega$. This gives the frequency of oscillations:

$$\Omega = \frac{3}{8}s\bar{\eta}^{-1}\sin(\Delta + \delta) - \frac{3}{2}\eta^{-1} \qquad \text{(S9)}$$

providing $s\sin(-\delta) > 4$, with $\bar{\eta}^{-2} = \eta^2 + \frac{1}{9}$ and $\tan(\delta) = \frac{\eta}{3}$. The parameter η is the nonlinear damping, and is expected to be small, so we can approximate $\bar{\eta} \approx \eta$ and $\delta \approx 0$.

In our experimental implementation the feedback phase shift Δ has a frequency dependent component from the filters in addition to the voltage controlled value ϕ. Over the tuning range of the oscillator this can be approximated as linear so that

$$\Delta \simeq \phi - c\Omega \qquad \text{(S10)}$$

where we find $c \simeq 1/53$. Equations (S9) and (S10) were used to construct the theory curves in Fig. 3c.

We can also analyze the stability of the steady state oscillations, and the effect of additional noise terms in the equation of motion. It is convenient to write Eqs. (S7) and (S8) in the general form

$$\frac{da}{dT} = f_a(a, \Delta) \tag{S11}$$

$$\frac{d\theta}{dT} = f_\theta(a, \Delta) \tag{S12}$$

and we generalize the feedback phase equation (S10) to

$$\Delta \simeq \phi - c \frac{d\theta}{dT} \tag{S13}$$

The equations for the stability analysis about a steady oscillation are

$$\frac{d\delta a}{dT} = \frac{\partial f_a}{\partial a} \delta a + \frac{\partial f_a}{\partial \Delta} \delta\Delta \tag{S14}$$

$$\frac{d\delta\theta}{dT} = \frac{\partial f_\theta}{\partial a} \delta a + \frac{\partial f_\theta}{\partial \Delta} \delta\Delta \tag{S15}$$

Using Eq. (S13) we can evaluate $\delta\Delta$ in terms of $\frac{d\delta\theta}{dT}$, and then calculate $\frac{d\delta\theta}{dT}$ in terms of δa from Eq. (S15). Substituting into Eq. (S14) then gives

$$\frac{d\delta a}{dT} = \left[\frac{\partial f_a}{\partial a} - c \frac{\partial f_a}{\partial \Delta} \frac{\frac{\partial f_\theta}{\partial a}}{1 + c \frac{\partial f_\theta}{\partial \Delta}} \right] \delta a \tag{S16}$$

The oscillations are stable (unstable) if the term in the braces is negative (positive). On the other hand the steady state amplitude-phase shift curve is determined by

$$\frac{da}{d\phi} = - \left[\frac{\partial f_a}{\partial a} - c \frac{\partial f_a}{\partial \Delta} \frac{\frac{\partial f_\theta}{\partial a}}{1 + c \frac{\partial f_\theta}{\partial \Delta}} \right]^{-1} \frac{\partial f_a}{\partial \Delta} \left(1 - \frac{c \frac{\partial f_\theta}{\partial \Delta}}{1 + c \frac{\partial f_\theta}{\partial \Delta}} \right) \tag{S17}$$

The quantity in the braces in Eqs. (S16) and (S17) is the same. Thus the change from stability to instability occurs when $\frac{da}{d\phi} = \infty$, i.e. at the "nose"' of the $a(\phi)$ curve. It is easy to check that $d\Omega/d\phi$ is also infinite here, so the instability can also be identified as the nose of the $\Omega(\phi)$ curve.

Various different noise sources may be important in the experiment, for example noise from the feedback amplifier or other electronic noise, and thermomechanical noise in the resonator. These can be modeled by adding appropriate stochastic terms to Eq. (S5). An

important noise term is likely to be phase fluctuations in the feedback loop, which can be modeled by adding a stochastic term to the feedback phase Δ, and it is particularly straightforward to analyze the effect of this term for frequency offsets from oscillator frequency small compared with the dissipative relaxation rate of the resonator.

The analysis for oscillator frequency fluctuations arising from noise in the feedback phase is similar. The equations for small fluctuations are the same as Eqs. (S14) and (S15), with δa, $\delta \theta$, $\delta \Delta$ now the stochastic fluctuations.

For frequency offsets from the oscillator frequency less than $\left(\frac{\partial f_a}{\partial a} \right)^{-1}$ we can ignore the time derivative term in Eq. (S14). This means we can calculate an explicit equation for the oscillator phase fluctuations

$$\frac{d\delta\theta}{dT} = \left(\frac{\partial f_a}{\partial a} \right)^{-1} \left[\frac{\partial f_\theta}{\partial \Delta} \frac{\partial f_a}{\partial a} - \frac{\partial f_\theta}{\partial a} \frac{\partial f_a}{\partial \Delta} \right] \delta\Delta = \frac{d\Omega}{d\Delta} \delta\Delta \qquad (S18)$$

The last equality follows by direct calculation, and is physically obvious since we are treating the magnitude as adiabatically following the feedback phase fluctuations. Thus, we see that for operating points where the $\Omega(\Delta)$ curve is flat, or, including the frequency dependent phase Eq. (S10), where $\Omega(\phi)$ is flat, there is no oscillator frequency fluctuations due to noise in the feedback phase. This result is analogous to that of Greywall and Yurke for an oscillator based on a nonlinear (Duffing) resonator with a direct drive feedback system at *f*, with the operating point chosen to be at the critical amplitude of the resonator for the onset of bistability.

III.   PFO applicability criterion

PFO architecture is not only restricted to the type of device shown in the present manuscript. This broad applicability makes this architecture very compelling. The criterion whether a particular resonator can be used with PFO topology is that it is possible to parametrically tune the natural frequency of the device more than twice the linewidth:

$$\left.\frac{\partial f}{\partial V}\right|_{V_{max}} \cdot V_{max} \cdot \frac{Q}{f_0} > 2 \qquad (S19)$$

Where V should be understood not only as voltage (as it is referred here) but in a more general way as the external variable, that tunes the device frequency. V_{max} represents the maximum voltage that can be applied to the device *in practice* – in general this is limited by considerations such as dielectric breakdown (relevant for the piezoelectric actuation employed in our work), the maximum tolerable device heating, input/output crosstalk, or similar effects. Q and f_0 are the quality factor and characteristic resonant frequency of the resonator, Q/f_0 being the linewidth of the device.

This criterion is a direct consequence of the theory for parametrically excited resonators, where it is known[S2] that the onset of instability occurs when the parametric drive is high enough as to compensate the linear damping term which, in turn, happens when the frequency is being tuned twice the linewidth. Another way of interpreting Eq. (S19) is that the maximum voltage you can apply to the device is higher than the parametric threshold voltage, defined by:

$$V_{th} = 2\frac{f_0}{Q} \Big/ \left.\frac{\partial f}{\partial V}\right|_{V_{th}} \qquad (S20)$$

We can define the following dimensionless parameter

$$\Re = \frac{1}{2}\left.\frac{\partial f}{\partial V}\right|_{V_{max}} \cdot V_{max} \cdot \frac{Q}{f_0} \qquad (S21)$$

and evaluate it for different devices. It represents the maximum frequency shift attainable for a given device, expressed in terms of number of resonant linewidths, at V_{max}. If, for a given device, we find $\Re$ to be higher than 1, it is then capable of being used to build a PFO. As the maximum voltage depends on the device itself, and the tunability also depends on the applied voltage, here we report some numbers obtained from a survey of state-of-the-art resonators, assuming voltages used in the literature.

Table S1 | Comparison of different resonators to be used with PFO topology

Device	Ref.	f_0 (MHz)	Q	V_{max} (V)	Tunability (kHz/V)	$\Re$
AlN bulk	[S3]	225	2000	10	Not reported, estimated ≈ 2	0.01
AlN bulk	-	2000	2000	10	Not reported, estimated ≈ 200	1
Si disk	[S4]	1150	10^4	10	1000	1
AlN beam	NA	105	850	10	35	3
AlN beam	-	15	1200	10	35	30
Si beam	[S5]	10	3600	10	10	45
CNTs	[S6]	50	100	10	4000	80
CNTs	[S7]	250	10^4	10	300	120
Graphene	[S7]	175	10^4	10	300	175
Graphene	[S8]	50	125	20	6000	300
Si_3N_4 beam	[S9]	8	10^5	20	10	2500

The compilation in Table S1 shows that it should be possible to implement PFOs with a majority of NEMS and MEMS oscillators reported in the literature. For traditional MEMS resonators this implies that it should be possible to improve oscillator stability down to the thermal noise limit. This has not been yet attained by any mechanical oscillator. In addition, given the fact that undesirable cross-talk is circumvented by the use of our proposed architecture, even the smallest and most challenging devices (CNTs, Graphene, etc.) should self-sustain oscillations when incorporated into PFO topology. This could have tremendous impact in fields of small scale frequency standards and mass sensing.

IV.   Parametric Feedback oscillation condition

An interesting question is for which values of the parameters space determining the system it is possible to attain the onset of self-sustained oscillations. For traditional oscillators with direct-drive feedback at *f*, such proper choice of parameters is determined by the 'Barkhausen criterion' [S10]. As we point out in the main text, this criterion does not apply to the PFO topology. Here we determine a new set of criteria to ensure oscillation in PFO by evaluating the parameter space within which it is possible to attain self-sustained oscillations. From Eq. (S5), we can derive the following two equations, analogous to (S7) and (S8):

$$-4 - \eta a^2 = F(|a|^2) \sin(\Delta) a^2 \tag{S22}$$

$$\Omega = \frac{1}{8} F(|a|^2) \cos(\Delta) a^2 + \frac{3}{8} a^2 \tag{S23}$$

Equation (S22) provides a general criterion required to sustain PFO oscillations, it implies that the feedback gain needs to be large enough so that its projection on the damping quadrature compensates both linear and non-linear damping. We first extract the oscillator frequency, which directly relates to the amplitude of oscillation, regardless of the feedback gain, in a similar manner to Eq. (S9) for saturated gain:

$$\Omega = -\left(\frac{1}{2} + \frac{1}{8}\eta a^2\right) \cot(\Delta) + \frac{3}{8} a^2 \tag{S24}$$

For a PFO, as has been pointed out in the paper, the self-sustained oscillating state can only be attained if the system is initially driven by an external "direct drive" source. The nature of that initial driving force is not restricted; for example, it can be sinusoidal (direct drive at the resonance frequency *f₀*), an impulse, a step function, etc. The requirement for such drive is simply to generate initial motion in the resonator that, after being amplified and passed through the nonlinear element, becomes sufficiently large to compensate the linear and nonlinear dissipation (similar to Eq. (S22)).

V.   Theoretical modeling of the mode-coupling feature

We now model the phenomenon giving rise to the local flattening of the frequency/phase curve (depicted in the inset to Fig. 3C of the main manuscript). We assume this arises when feedback to the oscillating mode is reduced by "spurious" absorption into a second spatial mode of the resonator that becomes directly driven when its frequency is resonant with the *2f* feedback. To model this phenomenon we introduce frequency-dependent decrease in the saturated feedback *s* through a resonant absorption term. This is achieved by replacing Eq. (S9) with a new term,

$$s \rightarrow s \left(1 - \frac{\lambda \left(\frac{f_2}{2Q_2} \right)^2}{(2f - f_2)^2 + \left(\frac{f_2}{2Q_2} \right)^2} \right) \tag{S25}$$

Here f_2, Q_2 are the resonant frequency and quality factor of the second mode, and λ a constant depending on the coupling of the drive system to this mode. In Fig. S2 we show the result of this expanded theoretical model, where the flattening feature can be observed around 16.25 MHz.
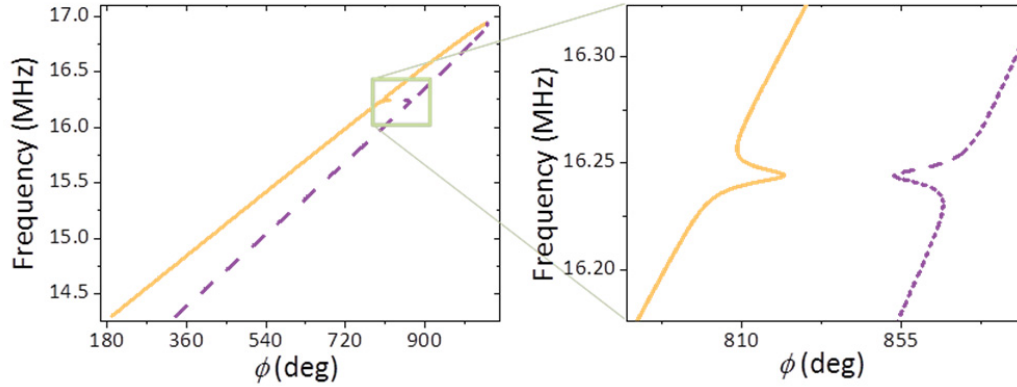
Fig. S2 | Theoretical prediction of the mode-coupling feature. Theoretical prediction of PFO frequency as a function of externally controlled phase shift including the effect of a second mechanical mode with a natural frequency around 32.5 MHz.

VI.   Experimental characterization of the nonlinear element

We experimentally characterize the transfer function of the nonlinear element in the feedback loop presented in Fig. 2 of the main manuscript. To do that, we send a signal to the nonlinear element at a frequency ω and monitor the power transferred at 2ω. The result is presented in Fig. S3.
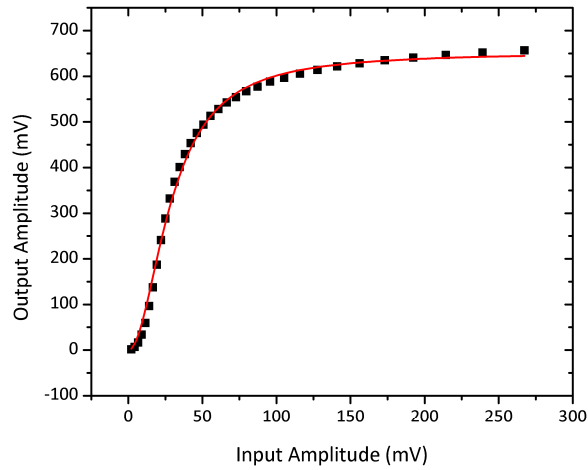

Fig. S3 | Transfer function of the nonlinear element. Experimental plot (scattered data) of the amplitude after the nonlinear element (monitored at 2ω) as a function of the input amplitude (at ω). Red line represents the nonlinear fitting of our experimental data to a function of the type described in Eq. (S3).

VII. Thermomechanical limit of the frequency stability

An important fundamental noise limit of any mechanical oscillator is set by its thermomechanical noise. If we consider a mechanical oscillator which in this limit, its *phase noise* can be estimated via Leeson's formula to be:

$$\mathfrak{L}(\Delta\omega) = 10 \log\left(\frac{k_B T}{E_{osc} Q} \frac{\omega_0}{\Delta\omega^2}\right)$$

(S26)

Here, we replot the results from Fig. 3D in the main paper together with the fundamental limit of the system in Fig. S4.
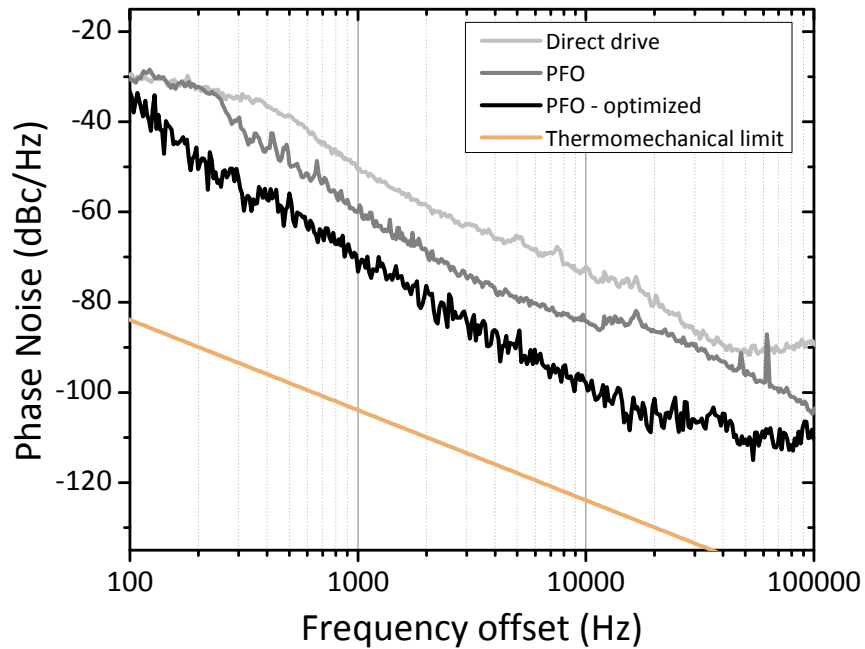
Fig. S4 | Phase noise comparison. Experimental phase noise measurements presented in the main paper and thermomechanical limit.

References

S1.   R. B. Karabalin *et al.*, Piezoelectric nanoelectromechanical resonators based on aluminum nitride thin films. *Applied Physics Letters* **95**, 103111 (2009).

S2.   R. Lifshitz, M. C. Cross, in *Reviews of nonlinear dynamics and complexity,* H. G. Schuster, Ed. (Wiley-VCH, Weinheim, 2008), vol. 1, chap. 1.

S3.   C. J. Zuo, N. Sinha, J. Van der Spiegel, G. Piazza, Multifrequency Pierce Oscillators Based on Piezoelectric AlN Contour-Mode MEMS Technology. *J Microelectromech S* **19**, 570 (2010).

S4.   J. Wang, Z. Y. Ren, C. T. C. Nguyen, 1.14-GHz self-aligned vibrating micromechanical disk resonator. *2003 Ieee Radio Frequency Integrated Circuits (Rfic) Symposium, Digest of Papers*, 335 (2003).

S5.   S. Lee, M. U. Demirci, C. T. C. Nguyen, A 10-MHz micromechanical resonator Pierce reference oscillator for communications. *Transducers '01: Eurosensors Xv, Digest of Technical Papers, Vols 1 and 2*, 1094 (2001).

S6.   B. Lassagne, Y. Tarakanov, J. Kinaret, D. Garcia-Sanchez, A. Bachtold, Coupling Mechanics to Charge Transport in Carbon Nanotube Mechanical Resonators. *Science* **325**, 1107 (2009).

S7.   A. Eichler *et al.*, Nonlinear damping in mechanical resonators made from carbon nanotubes and graphene. *Nat Nano* **6**, 339 (2011).

S8.   C. Y. Chen *et al.*, Performance of monolayer graphene nanomechanical resonators with electrical readout. *Nat. Nanotechnol.* **4**, 861 (2009).

S9.   Q. P. Unterreithmeier, E. M. Weig, J. P. Kotthaus, Universal transduction scheme for nanomechanical systems based on dielectric forces. *Nature* **458**, 1001 (2009).

S10.   A. Hajimiri, T. H. Lee, *The design of low noise oscillators* (Kluwer Academic Publishers, Boston, 1999).